Physicochem. Probl. Miner. Process., 60(1), 2024, 183655

http://www.journalssystem.com/ppmp

Physicochemical Problems of Mineral Processing

ISSN 1643-1049

Innovative correlation relating the destruction of graphite flakes to the morphology characteristics of minerals

Nailing Wang, Xinyang Xu, Yanxin Jiang, Zhitao Yuan, Jiwei Lu, Lixia Li, Qingyou Meng

School of Resources and Civil Engineering, Northeastern University, Shenyang 110819, Liaoning, China

Corresponding authors: xuxinyang@mail.neu.edu.cn (Xinyang Xu), lujiwei20041202@163.com (Jiwei Lu)

Abstract: The morphology characteristics (sphericity, roundness, and surface roughness) affecting the destruction of gangue minerals on graphite flakes during the grinding process were systematically analyzed. Coupled with MS and SEM, sphericity analysis showed that graphite was flaky, which was similar to muscovite but different from granulous quartz and albite, and the roundness of the four minerals from high to low was graphite, quartz, albite, and muscovite. AFM analysis showed that the surface roughness of graphite and muscovite was very low compared to that of quartz and albite (higher than quartz). The size and crystal integrity of graphite flakes were both destroyed by gangues during the grinding process, and the destruction of quartz and albite was serious compared to that of muscovite. Sphericity dominantly affected the destruction: the larger the sphericity, the more serious the destruction, which was also negatively related to roundness but positively related to surface roughness.

***Keywords*:** flaky graphite, dynamic particle morphology analyzer, sphericity, roundness, surface roughness

1. Introduction

Graphite (Mohs hardness 1-2) is one of the allotropes of the element carbon among diamond, lonsdaleite, fullerenes, and several non-crystalline forms (Barrenechea et al., 2009). It is one of the most versatile non-metallic minerals, which has some physicochemical properties of both metallic and nonmetallic materials such as conductivity, thermal conductivity, high-temperature resistance, high strength, thermal shock resistance, chemical stability, lubricity, and so on (Beyssac et al., 2002). Therefore, graphite is widely used in the traditional industrial field, such as conductive material in the electrical industry, refractory material in the metallurgical industry, lubricant in the mechanical industry, and corrosion-resistant material in the chemical industry (Shaji, 2022; Alberts, et al., 2009). At the same time, in the modern high-precision field, graphite can be mainly used to make natural graphite anode materials for lithium-ion batteries, isotropic graphite, expanded graphite, spherical graphite, graphene, and so on (Radoń et al., 2018; Tarannum et al., 2023; Vanderbruggen et al., 2021). Especially with the vigorous development of the electric vehicle industry and the popularity of lithium-ion batteries, the demand for graphite is huge and growing.

Natural graphite can be classified as crystalline graphite (flaky and lumpy) and cryptocrystalline graphite based on crystalline morphology (Qui et al., 2022; Xu et al., 2021). The particle size of crystal in flaky graphite is larger than 1 μm, while the large-flake graphite is greater than 0.15 mm (Peng et al., 2016; Shen et al., 2021). The shape of the graphite particles is very important for its utilization since particles with flaky shapes can maintain relatively high electrical and thermal conductance as well as lubrication ability, so the larger the flakes, the better the performance and the higher the economic value (Byoung et al., 2022).

It is precisely because of the excellent properties, high value, and non-renewability of large-flake graphite that it is necessary to maximize avoid reducing its destruction in the separation process, especially grinding. Based on this, traditional graphite beneficiation generally adopts a special process of stage grinding-stage flotation to reduce destruction. Therefore, exploring effective methods to protect the flake structure is the key and difficult spot for flaky graphite beneficiation, in particular, the effective

DOI: 10.37190/ppmp/183655

protection of flake structure during the grinding process. In recent years, mineral processing researchers have done a lot of meaningful study in the following aspects, such as grinding medium, grinding equipment, grinding technology, etc. (Long et al., 2013; Mu et al., 2020a; Mu et al., 2020b). Sun et al. (2017) proposed an approach of steel rod coarse grinding and pebble regrinding, which effectively reduced the destruction of graphite flakes and improved the grinding efficiency. In addition, a pre-screening process was applied to significantly improve the content of large flakes in the final concentrate. Long et al. (2022) carried out comparative experiments on four grinding media including steel balls, microcrystalline balls, brown ceramic balls, and pebbles for regrinding of rough graphite concentrate. The results showed that optimal graphite grinding and flotation indicators appeared with brown ceramic balls as the regrinding medium, in other words, the concentrate containing lower fine-grain flakes could be obtained, and its flake surface was smooth and its structure was more regular and complete. Ma et al. (2021) proposed a novel technology including a HPGR and a stirred mill as primary grinding techniques and a nanobubble flotation column as a separation process. The results showed that the process produced a concentrate with 94.82% carbon grade and 97.89% recovery from an open circuit of one rougher and two cleaner flotation stages. SEM microphotographs indicated that HPGR offered the advantage of more effective protection of graphite flakes during crushing. Grinding test results showed that stirred mills could not only protect graphite flakes but also promote the efficient liberation of graphite.

However, the destruction of gangue minerals on graphite flake structure during the grinding process was rarely studied. According to the mineralogy research and XRD analysis in relevant kinds of literature, the main gangue minerals of flaky graphite ore are silicate minerals such as quartz (Mohs hardness 7), feldspar (Mohs hardness 6-6.5), and mica (Mohs hardness 2.5-3), etc. (Cheng et al., 2017; He at al., 2017; Cen et al., 2018; Zhou and Cheng, 2016; Liu et al., 2022). Quartz (SiO_2) belongs to the trigonal system, and $[SiO_4]^{4-}$ tetrahedron is the basic structural unit. When a quarter of the Si^{4+} is replaced by Al^{3+} in quartz, which becomes feldspar (including potassium feldspar, albite, and anorthite, etc.), here we focus on albite ($Na_2O \cdot Al_2O_3 \cdot 6SiO_2$), which belongs to the triclinic system. Mica, a layered silicate mineral, mainly includes muscovite, biotite, phlogopite, and so on, here we focus on muscovite ($KAl_2(AlSi_3O_{10})(OH)_2$), which belongs to the monoclinic system.

Despite entrainment and hetero-coagulation with graphite in the flotation process, these gangue minerals would severely deteriorate the graphite flakes during the grinding process because of their high hardness compared to graphite (Liang et al., 2018; Li et al., 2014; Zhou et al., 2022). The graphite ore with high-hardness gangue minerals is difficult to comminute, which inevitably leads to the grinding time or stages increase. What's more, high-hardness gangue minerals will destroy the graphite flakes during the grinding process (Liu et al., 2014; Feng, 2015). In addition, the destructiont of gangue minerals on graphite flakes is also significantly affected by particle surface morphology characteristics (mainly including shape and roughness) besides hardness (Vaziri Hassas et al., 2016). The shape of particles is mainly determined by sphericity and roundness, while roughness is perhaps the most remarkable property of a solid surface (Sun et al., 2023; Guven et al., 2015). Sphericity signifies the similarity of the particle's overall shape to a sphere at the macroscale, and generally, on this scale, the particles are described as spherical, flat, and elongated. Roundness is the antonym of the term angularity and implies the particle's corners at the mesoscale. Finally, roughness shows the surface texture of the particle at the microscale (Ulusoy, 2023). To date, however, almost none of the research for destructive effects related to the surface morphology characteristics of gangue minerals has been developed. Thus, it is necessary to carry out a related study to find a breakthrough direction for protecting graphite flake structures.

In this work, we used three parameters: sphericity, roundness, and surface roughness to quantify the surface morphology characteristics significantly affecting the destruction of the three main gangue minerals including quartz, albite, and muscovite. These parameters would be systematically analyzed by Camsizer X2 dynamic particle morphology analyzer, molecular dynamics simulation (MS), scanning electron microscopy (SEM) analysis, and atomic force microscope (AFM) analysis. In addition, the destruction of different gangue minerals on graphite flakes will be investigated using grinding tests, particle size analysis, SEM-EDS analysis, and XRD patterns. Finally, the correlation between surface morphology characteristics parameters and destructive effects could be inferred. This work will provide a reference for selective grinding of flaky graphite ore to protect graphite flakes from destruction.

2. Materials and methods

2.1. Materials

The graphite, quartz, albite, and muscovite pure minerals used in this study were obtained from Jixi (Heilongjiang Province, China), Guangzhou (Guangdong Province, China), Feicheng (Shandong Province, China), and Shijiazhuang (Hebei Province, China), respectively. The laboratory-scale HPGR (Shenyang Shengshi Wuhuan Science and Technology Co., Ltd, China) was constructed to crush the high-grade graphite lump ore sample to −1 mm after handpicking. Then the comminution products were separated using shaking tables repeatedly to obtain pure graphite. In addition, the pure graphite mineral (fixed carbon 96%) was screened into the large flake size fraction (+0.15 mm) by a standard sieve. The gangue minerals quartz, albite, and muscovite directly obtained from ultrahigh grade rocks were broken to −2 mm using the roll crusher and then ground in the ceramic ball mill, respectively. The three gangues were all sieved into the same grain size as -1.0+0.075 mm. The X-ray diffraction (XRD) analysis of the four minerals in Fig. 1 shows that there were no other impurities in graphite, quartz, albite, and muscovite pure minerals.

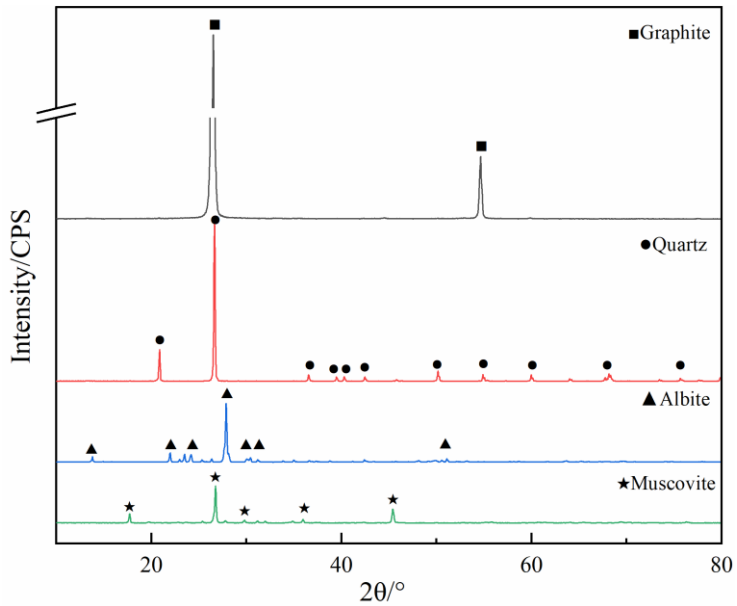

Fig. 1. XRD patterns of minerals

2.2. Methods

2.2.1. Grinding tests

The grinding tests were performed in QM-WX04 horizontal planetary ball mill (Nanjing University, China), which had four 40 mL stainless steel tanks with five 5 mm and thirty 3 mm ceramic balls (the main composition was Al_2O_3). 2.0 g pure graphite or mixture (1.0 g graphite and 1.0 g gangue mineral) were ground at 50% mass concentration at different durations (15, 30, 45, and 60 s) in each grinding test. The graphite (+0.15 mm) was sieved by a 0.15 mm stainless steel standard screen and weighed after grinding and separating from gangue minerals. Three tests were carried out for each grinding condition, and the average was used as the final result.

2.2.2. Molecular dynamics simulation

The molecular dynamics simulations in this work were carried out using Materials Studio V8.0 (Accelrys, USA). The models of graphite, quartz, albite, and muscovite were operated through the software package, and the mineral surfaces were optimized on the Materials Visualizer module.

2.2.3. Dynamic particle morphology analysis

The morphology of dynamic particles was determined using a Camsizer X2 dynamic particle morphology analyzer (Microtrac MRB, Germany), an optically based instrument capable of determining

grain size from 0.8 μm to 8 mm. The object and schematic diagram of the Camsizer X2 dynamic particle morphology analyzer is shown in Fig. 2. It has three modes (including free fall mode, air jet mode, and liquid flow mode) to disperse samples. In this measurement, free fall mode was used for the 1.0 g dry powders, that is, the dry particles free-fell and dispersed from a hopper to an analyzing area by a vibrating feeder, where they passed in front of two LED light sources. Camsizer X2 used dual cameras (basic camera for coarse particles and zoom camera for fine particles) to capture pictures (4.2 M pixel resolution) of falling particles at a rate of 300 frames per second. These huge images are analyzed in real time by Particle X-Plorer software, at the same time, particle size and shape parameters such as sphericity and roundness are accurately calculated (Czajkowska et al., 2015; Trubetskaya et al., 2016). The representative pictures for four minerals were selected according to the calculation results.

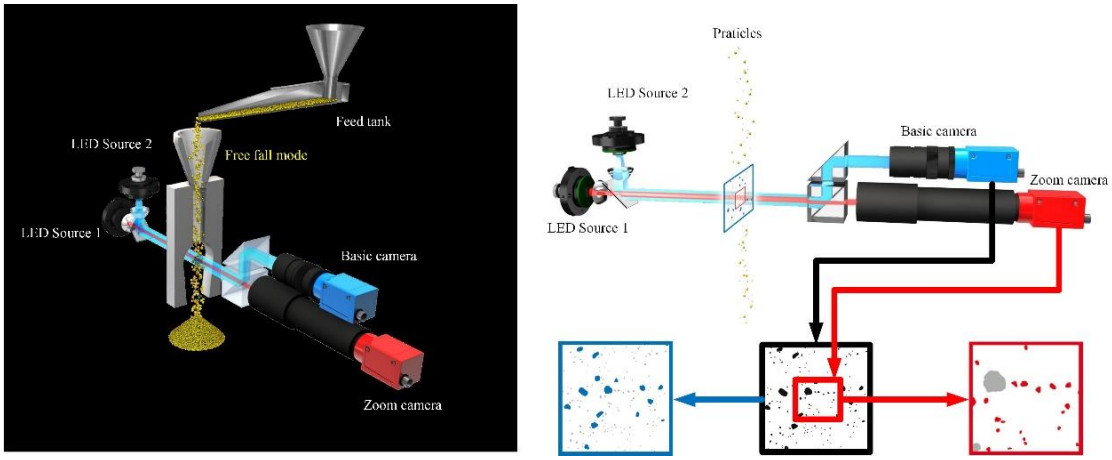

Fig. 2. Object and schematic diagram of Camsizer X2 dynamic particle morphology analyzer

Sphericity is the degree close to a sphere of a particle (Li and An, 2023; Zhang and Tahmasebi, 2023; Tophel et al., 2023; Zhang et al., 2023). The sphericity of a sphere is equal to 1, and the sphericity of any other shape particle is less than 1, that is, the closer the particle is to the sphere, the closer its sphericity is to 1 (Yao et al., 2022; You, 2022; Rodrigues et al., 2023). Sphericity is the ratio of the surface area of the same volume sphere (S) to the surface area of the particle itself (S_p), which is generally considered to be a shape descriptor for irregular particles (Yang et al., 2019). The sphericity of any particle can be calculated via the formula as follows:

$$\varphi = \frac{S}{S_p} = \frac{(36\pi V^2)^{1/3}}{S_p} \tag{1}$$

where φ is the sphericity of the particle, S is the area of the same volume sphere, S_p is the area of the particle, and V is the volume of the particle.

Roundness is the average curvature radius of all relevant corners divided by the largest inscribed circle radius. Roundness describes large undulations of the overall particle outline and expresses the sharpness of the particle corners, the larger the value, the fewer the edges and angles. It can be calculated via the formula as follows:

$$\psi = \sum(r_i/N)/r_{max} \tag{2}$$

where ψ is the roundness of the particle, r_i is the radius of the subcircle that is fitted to the i_{th} corner, and r_{max} is the radius of the maximum inscribed circle (Wu et al., 2021).

Sphericity and roundness are independent of each other, however, they are related in terms of describing particle morphology first developed by Krumbein (1941). The schematic illustration of definitions and relationships for sphericity and roundness are shown in Fig. 3.

2.2.4. SEM images and EDS analysis

A Gemini 300 (Zeiss, USA) scanning electron microscope (SEM) was used to observe the morphology of mineral particles. The graphite, quartz, albite, and muscovite pure minerals were dried at 45 degrees Celsius in a drying oven after grinding and sample-reducing by grid method. For SEM images, 5 individual images at different areas in the field of vision were randomly detected for each 10 mg mineral

sample, in which the representative images of the four minerals were selected after careful observation and comparison. In addition, the chemical elements distribution of graphite after grinding with different gangue minerals was detected by (energy dispersive spectrometry) EDS spectra, which were obtained in the range of −0.20 to 14 keV.

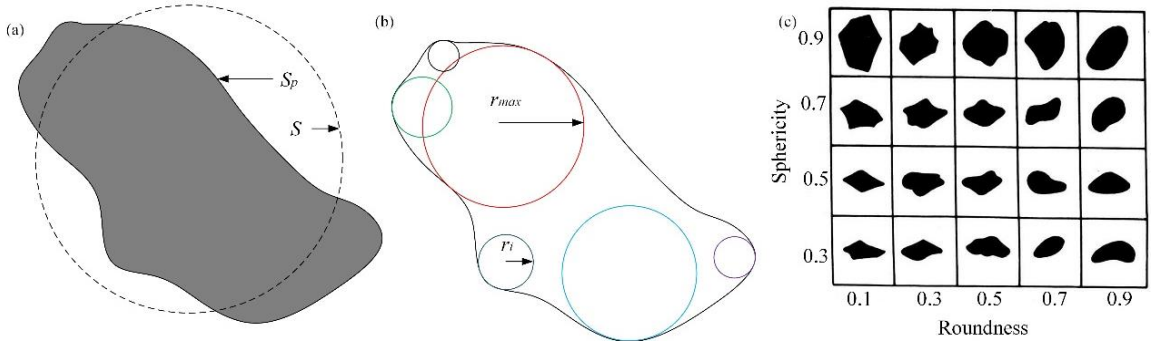

Fig. 3. Schematic illustration of definitions and relationship for sphericity and roundness (a: sphericity; b: roundness; c: relationship)

2.2.5. AFM analysis

The atomic force microscopy (AFM) images of mineral samples were captured using MultiMode 8 (Bruker, Germany) microscope to analyze the surface roughness. Before detection, the mineral samples were dispersed in a measuring glass with deionized water by an ultrasonic cleaning device for 10 min. A drop of the upper suspended liquid with mineral particles was dropped onto the clean mica substrate before drying in an oven. The AFM image is produced for 1.0×1.0 μm² when the scan size is set to 1 μm. Topography and data were post-processed using Nanoscope Analysis (v1.50). In this paper, 5-10 individual particles of each mineral were randomly detected to ensure representativeness (Li et al., 2019). The roughness values of the five images are calculated respectively, and the image closest to the average value is selected as the representative image.

2.2.6. Particle size distribution measurements

The particle size distributions of graphite before and after grinding were detected using a particle size analyzer Mastersizer 3000 (Malvern, UK). After grinding, the graphite was separated from gangue minerals by flotation and dried for measurements.

2.2.7. XRD measurements

XRD measurements were performed to identify the mineral composition of samples and the crystal structure of graphite before and after grinding with different gangue minerals. Ultima IV diffractometer (Rigaku, Japan) was used to carry out this investigation at a 10°/min scanning rate in the Bragg angle (2θ) range of 10°-80°. The collected data on mineral composition and crystal structure was further explored by comparing the crystal diffraction patterns using Jade 6 software.

3. Results and discussions

3.1. Morphology characteristics

3.1.1. Crystal structures

The structures of the optimized mineral crystals and lattice parameters of the four minerals were simulated by molecular dynamics simulation are shown in Fig. 4.

As shown in Fig. 4, the graphite crystals have a typical hexagonal lattice structure, the length of the C—C bond in basal plane surfaces is 1.42 Å, and the interplanar distance is 3.40 Å, respectively. Quartz has a similar crystal structure to albite, and they both belong to framework silicate minerals. When Al^{3+} replaced a quarter of the Si^{4+} in quartz structure, this part of [SiO_4] tetrahedron turned to [AlO_4] tetrahedron producing vacancies, which are dominated by long radius and low state Na^+ forming albite. Generally speaking, the bond strength of Al—O is lower than that of Si—O, so Al—O is easier to break. On the contrary, the crystal structure of quartz and albite is different from muscovite, which belongs to

layered silicate minerals and can completely cleavage along the interlayer (Xu et al., 2017). Moreover, the molecule structures and lattice parameters essentially affect the surface morphology characteristics of mineral particles.

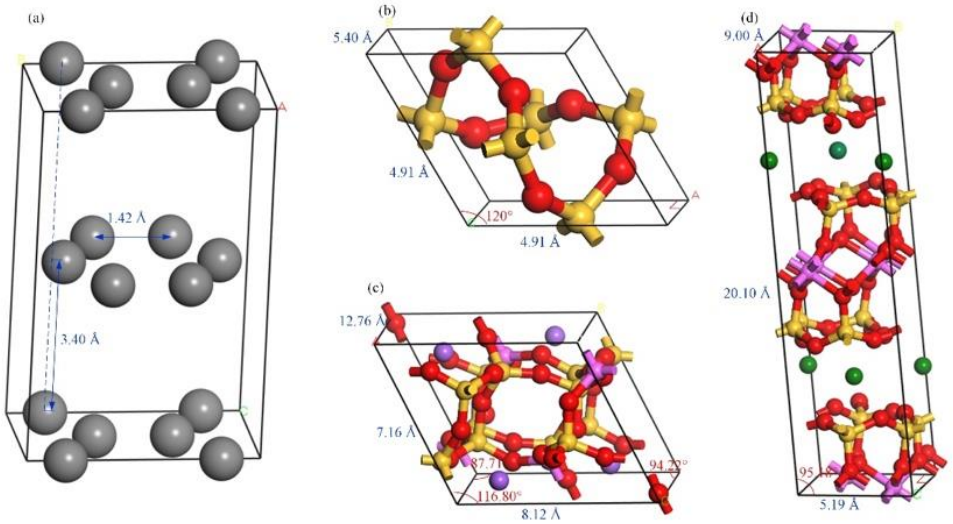

Fig. 4. Molecule structures of the four minerals (a: Graphite, b: Quartz, c: Albite, d: Muscovite) (Gray: C; Yellow: Si; Red: O; Pink: Al; Purple: Na; Green: K)

3.1.2. Dynamic particle morphology analysis

Sphericity and roundness, as two surface morphology characteristics of mineral particles, were detected and calculated through thousands of images captured by the Camsizer X2 dynamic particle morphology analyzer. The representative images are shown in Fig. 5, and the sphericity and roundness values calculated by the software are shown in Table 1. The standard deviations of sphericity for graphite, quartz, albite, and muscovite calculated from the original data in the test report are 0.056, 0.043, 0.036, and 0.063, respectively.

Table 1. Sphericity and roundness of the four minerals

Minerals	Graphite	Quartz	Albite	Muscovite
Sphericity	0.5939	0.6975	0.6965	0.5549
Roundness	0.3907	0.3804	0.3444	0.2007

Table 1 presented the sphericity of graphite and muscovite were both lower than that of quartz and albite, indicating that they were far away from the sphere, while the roundness of graphite was higher than that of muscovite, manifesting that muscovite had more edges and angles comparing to graphite. Corresponding to Fig. 4 (c), graphite and muscovite both belonged to the flaky minerals, just as Fig. 5 (a) and (d) appeared, that was because there were complete cleavage planes in the two minerals crystal. The sphericity of quartz and albite were 0.6975 and 0.6965, showing that quartz and albite were similarly granulous and closer to a sphere referencing Fig. 4 (c), which were consistent with the images in Fig. 5 (b) and (c). At the same time, the roundness of quartz and albite were 0.3804 and 0.3444, expressing that albite particles had more edges and angles compared to quartz.

In short, according to sphericity, quartz, and albite were similar granulous, which were very different from graphite. On the contrary, muscovite had a flaky structure similar to graphite. In addition, the number of edges and angles from less to more as flows: graphite, quartz, albite, and muscovite on the base of roundness. The results were consistent with previous theoretical MS.

3.1.3. SEM analysis

SEM analysis was carried out to observe the morphology of the four minerals more directly. The typical images and the size of representative particles of the four minerals at the same magnification (100×) are shown in Fig. 6.

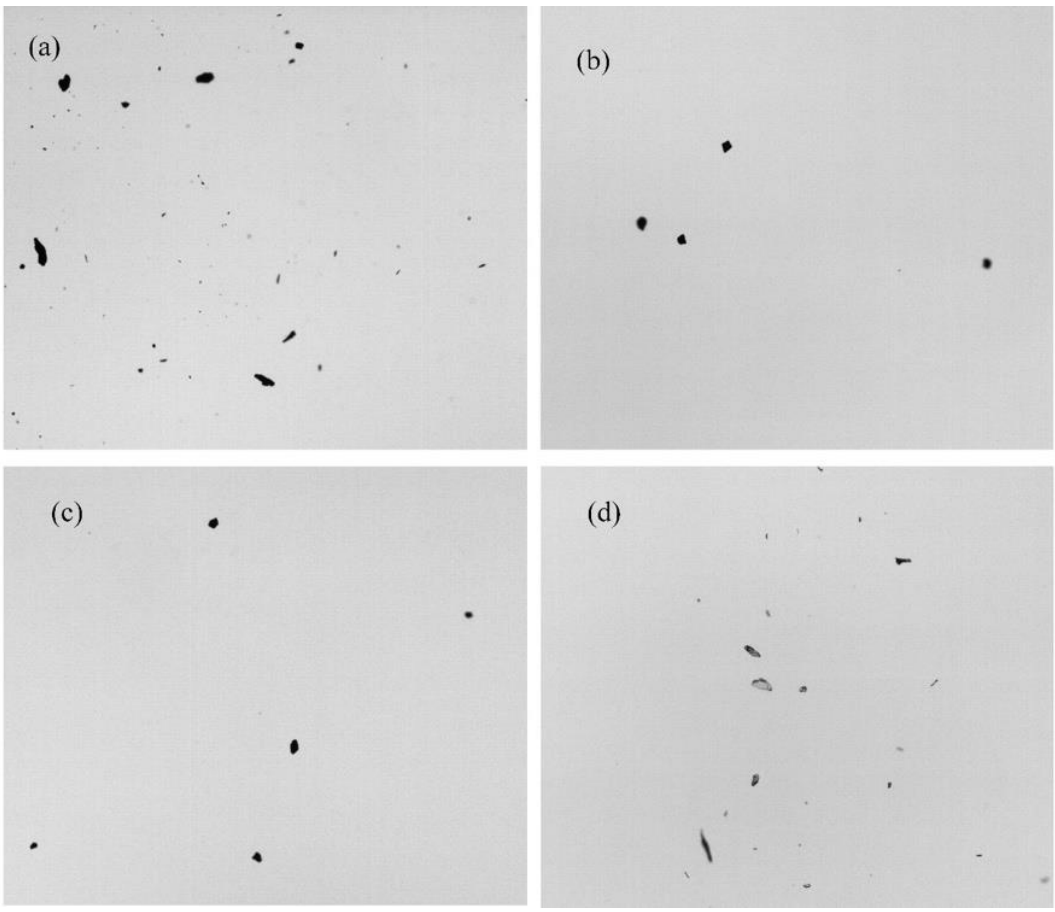

Fig. 5. Representative images of the four minerals by Camsizer X2 (a: Graphite, b: Quartz, c: Albite, d: Muscovite)

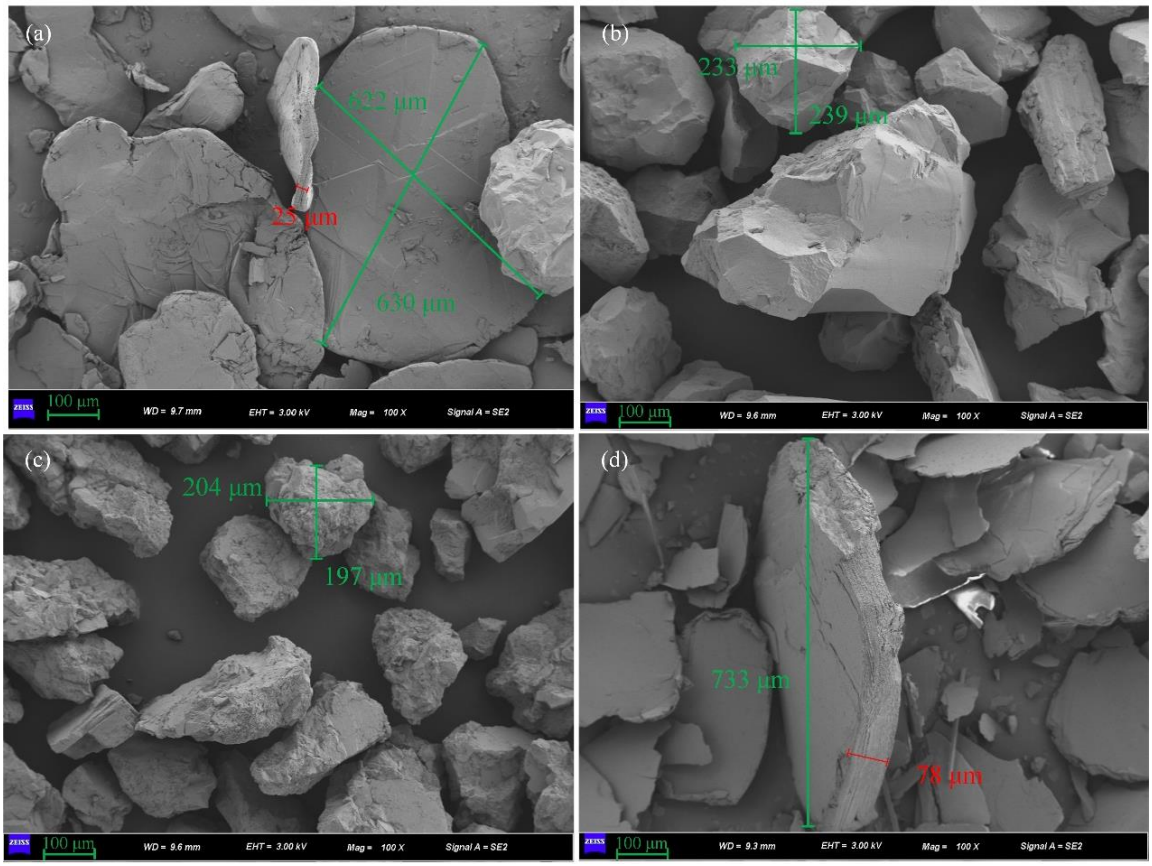

Fig. 6. SEM images of the four minerals (a: Graphite, b: Quartz, c: Albite, d: Muscovite)

On the whole, graphite and muscovite particles are both flaky, while quartz and albite particles are both granular as shown in Fig. 6. Comparing diagrams (a) and (d), it can be seen that graphite flakes are generally round or oval (A graphite flake has a diameter of 622×630 μm and a thickness of 25 μm), while muscovite are irregular flakes (A muscovite flake has a diameter of 733 μm and a thickness of 75 μm). In addition, the grain edges of graphite particles are much smoother than muscovite. Comparing diagrams (b) and (c), it can be seen that the surfaces of albite particles are relatively rougher than those of quartz. The SEM images strongly supported the viewpoint of dynamic particle morphology analysis intuitively.

It is worth noting that it can also be observed in the pictures that the complete cleavage plane of graphite and muscovite were both very slippy compared to the rough surfaces of albite and quartz. More advanced atomic force microscopes (AFM) will be used for microscopic observations to further research the surface roughness of the particles.

3.1.4. Surface roughness analysis

Generally, average roughness (R_a) and the root mean square roughness (R_q) were extracted to characterize the surface roughness of the particles (Alharbi et al., 2022). Besides, the dark color and light color of the images represent low and high sites on the surface, respectively (Lu et al., 2022). The representative two-dimensional (2D) AFM images for 1.0×1.0 μm² of particles are shown in Fig. 7, and the corresponding R_a parameter and R_q parameter of surfaces are shown in Table 2. The standard deviations of R_a and R_q for graphite, quartz, albite, and muscovite calculated from roughness values corresponding to the AFM images are 0.12 and 0.22, 3.75 and 4.78, 6.03 and 6.19, 0.13 and 0.30, respectively.

Table 2. The R_a and R_q parameters of the four minerals /nm

Minerals	R_a	R_q
Graphite	0.48	0.60
Quartz	33.7	48.3
Albite	41.1	54.5
Muscovite	0.92	1.39

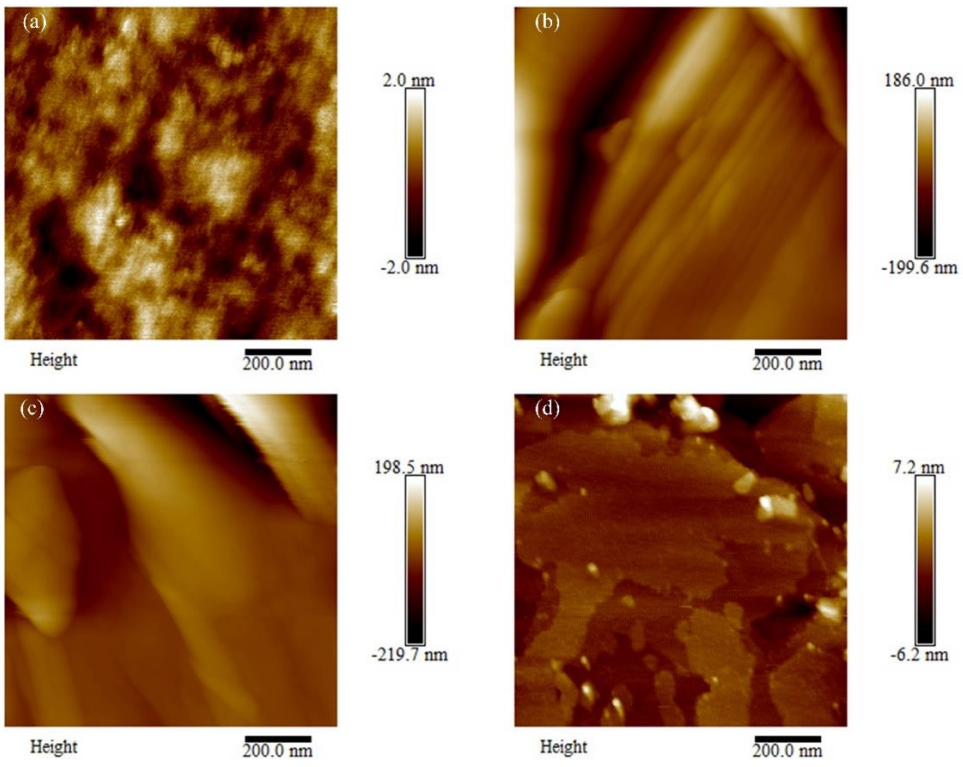

Fig. 7. 2D AFM images of the four minerals (a: Graphite, b: Quartz, c: Albite, d: Muscovite)

As depicted in Fig. 7, the morphology of graphite and muscovite looked smooth while the morphology of quartz and albite looked rugged in general. The maximum height difference of the four minerals was quite different, resulting in the light and dark distribution being discriminatory. The maximum height difference on the graphite and muscovite surfaces was just 4.0 nm and 13.4 nm, indicating that the surfaces of the two minerals were both flat, which fit well with the Ra and Rq parameters in Table 2. By contrast, the maximum height difference between quartz and albite were as much as 385.6 nm and 418.2 nm, respectively, illustrating that the surface of albite was more uneven than that of quartz, which is also consistent with the Ra and Rq parameters presented in Table 2. In a word, the AFM results exhibited obvious surface roughness discrepancy of the four mineral surfaces, that is, the surface roughness of graphite and muscovite were very low compared to quartz and albite, while the surface roughness of albite was relatively higher than quartz, which was in good agreement with the SEM images.

It can be concluded that quartz and albite were granulous, which was different from the flaky structure of graphite and muscovite according to sphericity analysis and SEM images. Besides, the roundness of the four minerals from high to low was as fllows: graphite, quartz, albite, and muscovite. AFM analysis further confirmed that the surface roughness of graphite and muscovite was quite low compared to those of quartz and albite. The contact modes and forces between three gangue particles and graphite particles applied in the mill are shown as the schematic diagram in Fig. 8. The contact mode between flaky graphite and flaky muscovite is close to face contact with tiny contact force, while the contact mode between flaky graphite and granulous quartz and albite is line contact or even point contact. Because of its lower roundness and higher roughness, the contact area between albite and graphite is smaller and the contact force per unit area is larger than that of quartz.

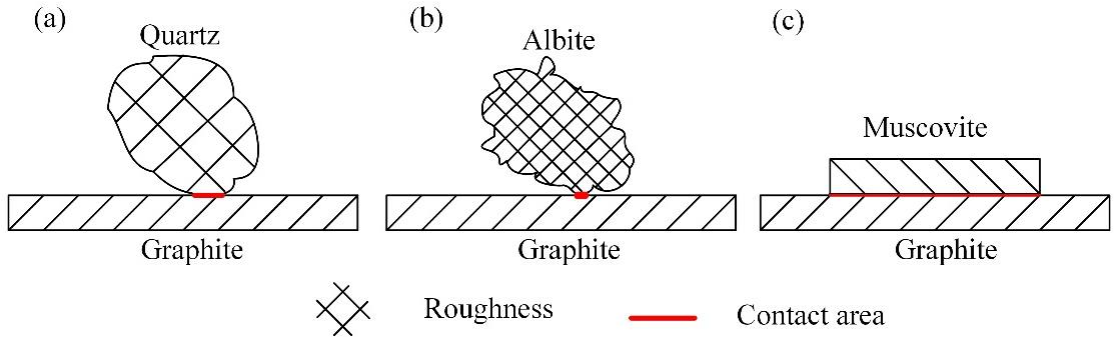

Fig. 8. Schematic diagram of contact mode and force between gangues and graphite during grinding

3.2. Destruction of gangue minerals on graphite flakes during the grinding process

The destruction of gangue minerals with different surface morphology characteristics on graphite flakes during the grinding process will be studied using grinding tests and the following detection methods.

3.2.1. +0.15 mm contents of graphite after grinding with different gangue minerals

The +0.15 mm graphite content in the Y-axis of the figure was the mass ratio of +0.15 mm graphite after to before grinding, and the higher the value, the less the destruction. The +0.15 mm contents of graphite after grinding with different gangue minerals were shown in Fig. 9.

As shown in Fig.9, the +0.15 mm contents of graphite after grinding with no gangue or three gangue minerals all declined with the grinding duration increasing, but the decline magnitudes were different. The downward trend of graphite after grinding with muscovite (from 85.50% to 67.02%) was slightly lower than that of grinding with no gangue (from 87.50% to 70.65%), illustrating that the presence of muscovite had little destruction on graphite flake. The downward trend of graphite after grinding with quartz (from 76.67% to 54.84%) is similar to that of grinding with albite (from 74.15% to 49.44%), while the +0.15 mm graphite content of grinding with albite was lower than that of quartz, indicating that the destruction of quartz was moderated than albite. In addition, the margin values of +0.15 mm graphite content between grinding with quartz or albite and grinding with no gangue increased gradually with the grinding duration increasing, revealing that the longer the grinding duration, the more severe the destruction for graphite.

In a word, compared with the destruction on graphite flake of quartz and albite, the destruction of muscovite was minimal, while the destruction of albite was slightly more intense than that of quartz. On the base of +0.15 mm contents of graphite, the particle size distributions of graphite after grinding with different gangue minerals will be further measured.

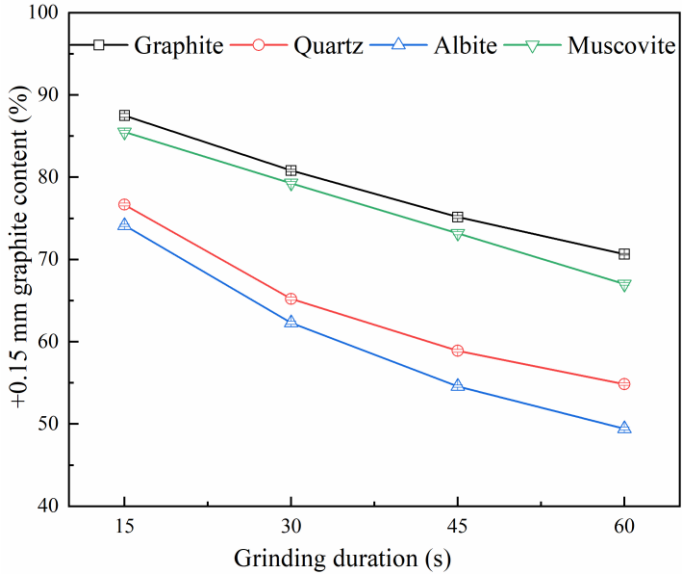

Fig. 9. +0.15 mm contents of graphite after grinding with different gangue minerals

3.2.2. Particle size distribution after grinding with different gangue minerals

The particle size distribution curves of graphite after grinding with no gangue or with quartz, albite, and muscovite at the ratio of 1:1 are plotted in Fig. 10, and particle size percentage results of D_{10}, D_{50}, and D_{90} are shown in Table 3.

As shown in Table 3, the D_{10}, D_{50}, and D_{90} sizes all decreased gradually after grinding with no gangue, with muscovite, with quartz, and with albite, respectively. It can be seen in Fig. 10 that the curves of graphite grinding with no gangue and with muscovite almost coincided, although the fine size percentage of the former was a little less than that of the latter. The coarse size peak sharply shifted down after grinding with quartz and albite, the peak value of quartz was higher than that of albite. Thus, the order of particle size from coarse to fine was as follows: graphite grinding with no gangue, with muscovite, with quartz, and with albite, declaring that the destructive effect of muscovite, quartz, and albite was gradually serious. The particle size distribution results were the same as the +0.15 mm graphite content of the grinding test above.

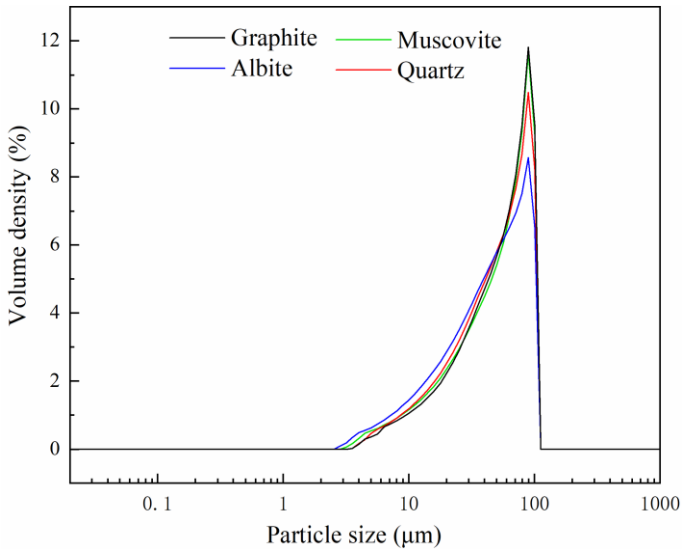

Fig. 10. The particle size distributions after grinding with different gangue minerals

Table 3. The particle size percentage/μm

Grinding condition	Particle size percentage		
	D_{10}	D_{50}	D_{90}
Graphite	14.647	52.426	88.977
Quartz	12.469	48.579	87.741
Albite	10.986	42.944	85.429
Muscovite	14.059	51.290	88.739

3.2.3. Morphology and size of particles after grinding with different gangue minerals

SEM-EDS analysis was used to gain better insight into the surface morphology of mineral surfaces after grinding. The results are shown in Fig. 11.

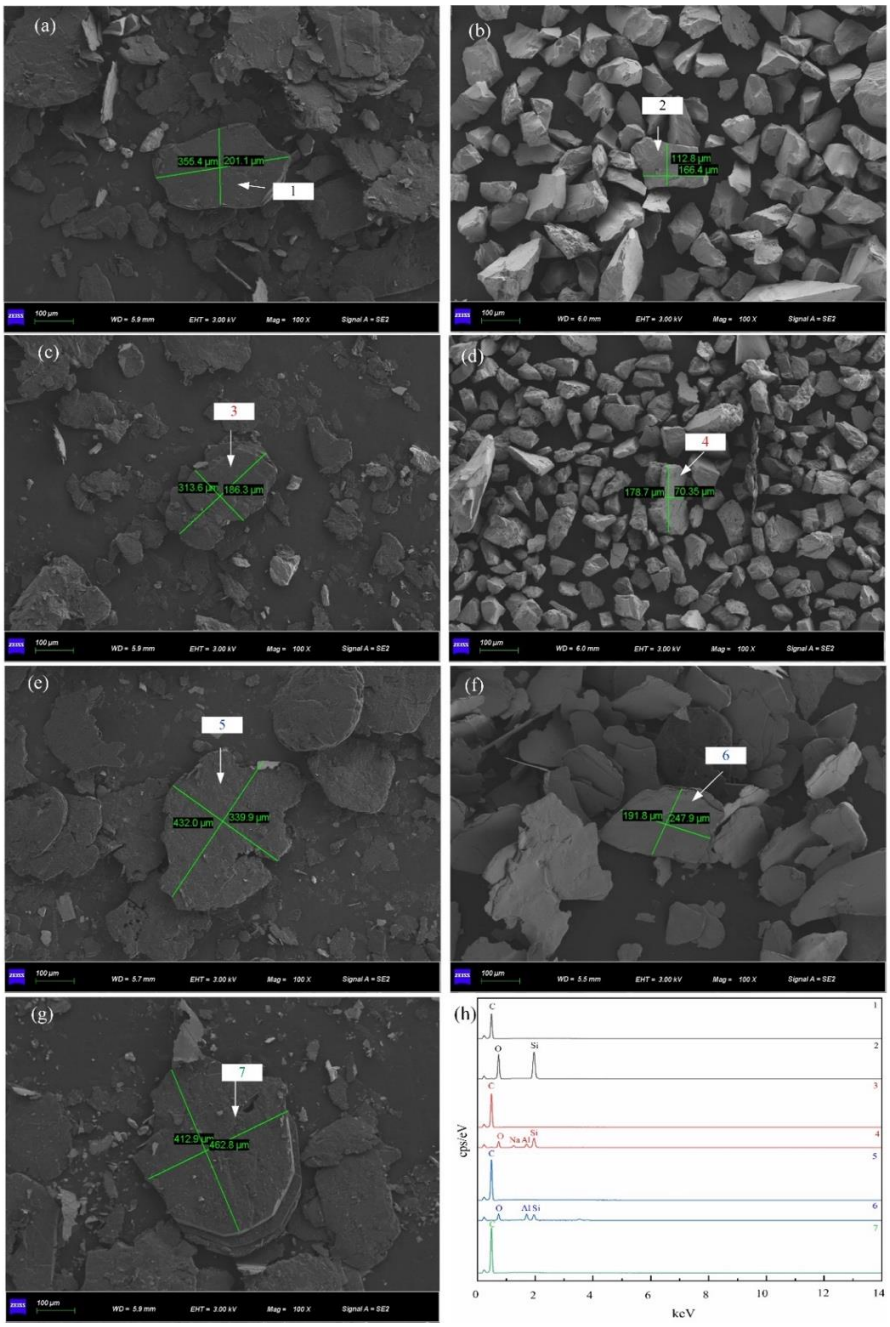

Fig. 11. SEM images and EDS spectra of minerals after grinding (a: graphite grinding with quartz; b: quartz grinding with graphite; c: graphite grinding with albite; d: albite grinding with graphite; e: graphite grinding with muscovite; f: muscovite grinding with graphite; g: graphite grinding with no gangue; h: EDS spectra)

The EDS spectra (Fig. 11 (h)) depicted the chemical composition of each corresponding marked point. Four points of 1, 3, 5, and 7 on graphite flakes after grinding with different gangues contained only C element. The elements contained by point 2 of quartz, point 4 of albite, and point 6 of muscovite all fitted with the chemical formula of each mineral, indicating that these minerals were completely separated from graphite.

The micrographs of graphite surfaces showed clear differences before and after grinding: compared with graphite before grinding (diameter of 622×630 μm in Fig. 6 (a)), the graphite flakes all appeared with different degrees of destruction after grinding with different gangue minerals. Graphite flakes were very smooth and clean before grinding, whereas the flakes became smaller and a lot of debris appeared after grinding. The overall particle sizes were consistent with the measured representative maximum particle size. The particle size order from large to small was as follows: grinding with no gangue (diameter of 412.9×462.8 μm in Fig. 11 (g)), grinding with muscovite (diameter of 339.9×432.0 μm in Fig. 11 (e)), grinding with quartz (diameter of 201.1×355.4 μm in Fig. 11 (a)), and grinding with albite (diameter of 186.3×313.6 μm in Fig. 11 (c)). At the same time, the amount of debris also increased in turn. By comparing Fig. 11 (b) to Fig.6 (b), Fig. 11 (d) to Fig. 6 (c), and Fig. 11 (f) to Fig. 6 (d), it is found that the size of quartz, albite and muscovite particles also deceased than before grinding. The results visually proved that the destruction of muscovite, quartz, and albite on graphite flakes gradually became severe, which was a strong support for the above results of +0.15 mm contents of graphite and particle size distribution analysis after grinding tests.

3.2.4. XRD characteristic peaks of graphite after grinding with different gangue minerals

XRD study was then conducted to further prove the change in graphite crystal integrity. The results are shown in Fig. 12.

It can be seen from Fig. 12, the XRD diffraction peak shapes of four kinds of graphite were similar, which contained (002) and (004) characteristic peaks. Referring to the XRD pattern of pure graphite in Fig. 1, (002) and (004) characteristic peaks appeared at 2θ of 26.52 and 54.64, respectively. The (002) and

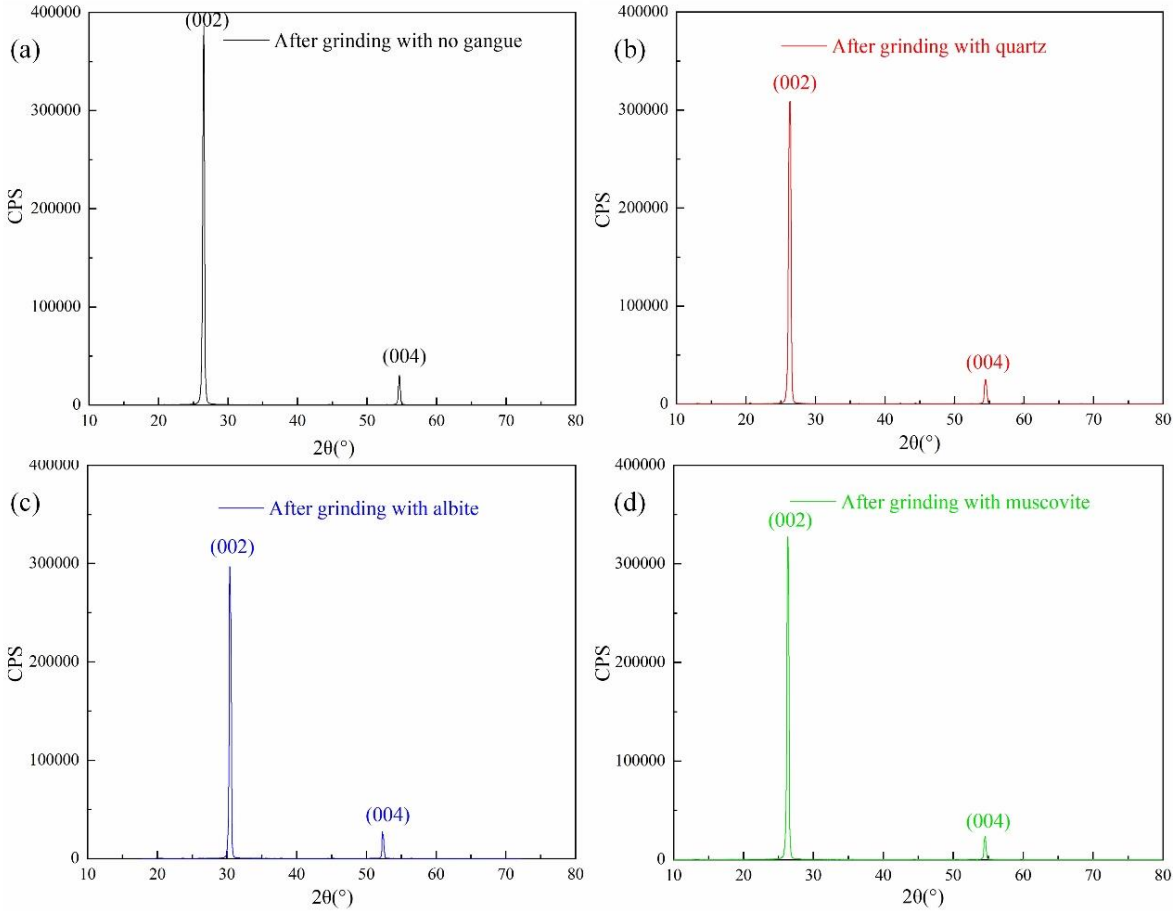

Fig. 12. XRD characteristic peak of graphite after grinding with different gangue minerals

(004) characteristic peaks of graphite after grinding with no gangue also appeared at 2θ of 26.52 and 54.64, but the intensity of diffraction peak slightly decreased than before grinding. The (002) and (004) characteristic peaks of graphite after grinding with quartz, albite, and muscovite appeared at 2θ of 26.32 and 54.44, 26.34 and 54.58, 26.2 and 54.54, respectively. Compared with graphite before grinding, the diffraction peaks of graphite after grinding with gangue minerals all shifted to the left. The order of (002) characteristic peak intensity from big to small was as follows: after grinding with no gangue, after grinding with no gangue, after grinding with muscovite, after grinding with quartz, and after grinding with albite, which all weaken than before grinding. The reasons for the decrease and left shift of peak intensity were due to the reduction of graphite flake size and the decrease of crystal integrity (Cheng et al., 2018). The results showed that the graphite crystal structures were seriously damaged after grinding with gangue minerals.

It can be concluded that the destruction of muscovite, quartz, and albite on graphite flake structures is gradually serious. In addition to the reduction of graphite flake size, the crystal integrity of graphite is also destroyed after grinding with gangue minerals.

3.3. The correlation between surface morphology characteristics and destruction

According to the above test and detection results, the destruction of albite on graphite flake structures was slightly more serious than that of quartz, while the destruction of muscovite was far weaker than that of quartz and albite. On this basis, the correlation between the three morphology characteristics parameters (sphericity, roundness, and surface roughness) and destruction could be inferred. Firstly, based on the great destruction differences between muscovite and the other two minerals, sphericity was the primary factor among them. The smaller the sphericity, in other words, the closer the gangue shape to the flaky graphite, the less the destruction. After that, the impact of roundness and surface roughness could be identified in turn by comparing the destruction of quartz and albite. Although with almost the same sphericity, the destruction of albite on graphite flake structures was slightly more serious than that of quartz, this is precisely because the roundness of albite was lower than that of quartz while its surface roughness was higher than that of quartz. It could be concluded that the roundness was negative to the destruction but the surface roughness was positive.

4. Conclusions

According to sphericity results, different from the flaky graphite and muscovite, quartz and albite were granulous. Besides, quartz had higher roundness and lower surface roughness compared with albite. These Gangues reduce the size and destroy the crystal integrity of graphite flakes during grinding, and the destructions of albite and quartz were serious than that of muscovite.

In conclusion, the larger the sphericity, the greater the destruction. In addition, roundness and surface roughness were negatively and positively correlated with the destruction, respectively. Therefore, it is very necessary to separate graphite from gangues (especially quartz and albite) as early as possible to avoid the destruction on graphite flakes during grinding for flaky graphite ores.

Acknowledgments

The authors would like to thank the National Key Research and Development Program of China (Grant No. 2020YFC1909601), the Fundamental Research Funds for the Central Universities (No. N2201010), and the National Natural Science Foundation of China (Nos. 51704057 and 52174243) and for financial support.

References

ALBERTS M., KALAITZIDOU K., MELKOTE S. 2009, *An investigation of graphite nanoplatelets as lubricant in grinding.* International Journal of Machine Tools and Manufacture, 49, 966-970.

ALHARBI N., TEERAKANOK S., SATTERTHWAITE J.D. ET AL. 2022, *Quantitative nano-mechanical mapping AFM-based method for elastic modulus and surface roughness measurements of model polymer infiltrated ceramics.* Dent Mater 38, 935-945.

BARRENECHEA J.F., LUQUE F.J., MILLWARD D. ET AL. 2022, *Graphite morphologies from the Borrowdale deposit (NW England, UK): Raman and SIMS data*. Contributions to Mineralogy and Petrology 2009; 158: 37-51

BEYSSAC O., GOFFE B., CHOPIN C. ET AL. *Raman spectra of carbonaceous material in metasediments: a new geothermometer*. Journal of Metamorphic Geology, 20, 859-871.

BYOUNG G.K., SANG K.C., HUN S.C. ET AL. 2022, *Grinding characteristics of crystalline graphite in a low-pressure attrition system.* Powder Technology, 126, 22– 27.

CEN D., ZHANG T., YU Y. ET AL. 2018, E*xperimental research on extraction and purification of large flake graphite from graphite ore in Heilongjiang*. Metal Mine., 504, 89-93.

CHENG X., PENG D., MU Y. ET AL. 2018, *Preparation and characterization of graphene by electrochemical stripping*. Journal of Zhongyuan University of Technology, 29, 23-26, 70.

CHENG F., ZHANG T., YU Y. ET AL. 2017, *Experimental research on beneficiation of large flake graphite ore in Madagascar*. Non-Metallic Mines, 40, 76-78.

CZAJKOWSKA M., SZNITOWSKA M., KLEINEBUDDE P. 2015, *Determination of coating thickness of minitablets and pellets by dynamic image analysis.* International Journal of Pharmaceutics, 495, 347-353.

FENG Y. 2015, *Study on regrinding technology and flotation rate of flake graphite.* Wuhan: Wuhan University Technology.

GUVEN O., CELIK M.S., DRELICH J.W. 2015, *Flotation of methylated roughened glass particles and analysis of particle–bubble energy barrier*. Minerals Engineering, 79, 125-132.

HE F., ZHANG L., QIU Y. ET AL. 2017, *Experimental esearch on Beneficiation of Large Flake Graphite in Eastern Area of Mozambique.* Bulletin of the Chinese Ceramic Society, 36, 4205-4210, 4216.

KRUMBEIN W.C. 1941, *Measurement and geological significance of shape and roundness of sedimentary particles.* Journal of Sedimentary Petrology, 11, 64-72.

LIANG L., ZHANG T., PENG Y. ET AL. 2018, I*nhibiting heterocoagulation between microcrystalline graphite and quartz by pH modification and sodium hexametaphosphate*. Colloids and Surfaces A: Physicochemical and Engineering Aspects, 553, 149-154.

LI M., AN X. 2023, M*ixing characteristics and flow behaviors of different shaped tetrahedra in a rotary drum: A numerical study.* Powder Technology, 417, 118262.

LI, H. FENG Q., YANG S. ET AL. 2014, *The entrainment behaviour of sericite in microcrystalline graphite flotation.* International Journal of Mineral Processing, 127, 1-9.

LI L., ZHANG C., YUAN Z. ET AL. 2019, *AFM and DFT study of depression of hematite in oleate-starch-hematite flotation system.* Applied Surface Science 480, 749-758.

LIU L., GUO L., SUN H. ET AL. *Comparative study on flotation technology of crystalline graphite from Akesai in Gansu Province.* Non-Metallic Mines 2022; 43(56-59), 63.

LIU X., ZHANG L., LI X. 2014, *Beneficiation experiment of a graphite in Luobei of Heilongjiang Province.* Metal Mine., 5, 105-109.

LONG Y., ZHANG, G. LI Z. 2013, R*esearch Progress of the Protecting Large Flaky Graphite*. China Non-matallic Minerals Industry, 2, 44-47.

LONG, Y., ZHANG G., XIAO X. ET AL. 2022, C*omparative experrmental research of media for graphitte regrinding*. Mining and Metallurgical Engineering, 42, 51-57.

LU J., WANG N., YUAN Z. ET AL. 2022, *The effects of ultrasonic wave on heterogeneous coagulation and flotation separation of pentlandite-serpentine.* Minerals Engineering, 188, 107828.

LUO X., LIN Q., WANG Y. ET AL. 2020, *New insights into the activation mechanism of calcium species to quartz: ToF-SIMS and AFM investigation.* Minerals Engineering, 153, 106398.

MA F., TAO D., TAO Y. ET AL. 2021, *An innovative flake graphite upgrading process based on HPGR, stirred grinding mill, and nanobubble column flotation*. International Journal of Mining Science and Technology, DOI: 10.1016/j.ijmst.2021.06.005.

MU Y., CHENG Y., PENG Y. 2020A, *The interaction of grinding media and collector in pyrite flotation at alkaline pH.* Minerals Engineering, 152, 106344.

MU Y., CHENG Y., PENG Y. 2020b, T*he interaction between grinding media and collector in pyrite flotation at neutral and slightly acidic pH.* Minerals Engineering, 145, 106063

PENG W., LI H., HU Y. ET AL. 2016, *Characterisation of reduced graphene oxides prepared from natural flaky, lump and amorphous graphites.* Materials Research Bulletin, 78, 119-127.

QIU Y., MAO Z., SUN K. ET AL. 2022, *Cost-efficient clean flotation of amorphous graphite using water-in-oil kerosene emulsion as a novel collector.* Advanced Powder Technology, 33, 103770.

RADOŃ A., WŁODARCZYK P., ŁUKOWIEC D. 2018, *Structure, temperature and frequency dependent electrical conductivity of oxidized and reduced electrochemically exfoliated graphite.* Physica E: Low-dimensional Systems and Nanostructures, 99, 82-90.

RODRIGUES S. J., HUGET N. V., T. RICHTER ET AL. 2023, *Influence of particle shape on tortuosity of non-spherical particle packed beds*. Processes, 1, 413-426.

SHAJI S.V.R. 2022, *An investigation on surface grinding using graphite as lubricant.* International Journal of Machine Tools & Manufacture, 42, 733–740.

SHEN K., CAO X., HUANG Z.-H. ET AL. 2021, *Microstructure and thermal expansion behavior of natural microcrystalline graphite*. Carbon, 77, 90-96.

SUN Y., BU X., ULUSOY U. ET AL. 2023, *Effect of surface roughness on particle-bubble interaction: A critical review. Minerals Engineering*, 201, 108223.

SUN K.K., QIU Y.S., ZHANG L.Y. 2017, *Preserving Flake Size in an African Flake Graphite Ore Beneficiation Using a Modified Grinding and Pre-Screening Process.* Minerals, 7

TARANNUM F., DANAYAT S., NAYAL A. ET AL. 2023, *Thermally expanded graphite polyetherimide composite with superior electrical and thermal conductivity.* Materials Chemistry and Physics, 298, 127404.

TOPHEL A., DUTTA T.T., OTSUBO M. ET AL. 2023, *Machine learning models to estimate stress wave velocities of cohesionless soils during triaxial compression influenced by particle characteristics.* Soil Dynamics and Earthquake Engineering, 165, 107649.

TRUBETSKAYA A., JENSEN P.A., JENSEN A.D. ET AL. 2016, *Comparison of high temperature chars of wheat straw and rice husk with respect to chemistry, morphology and reactivity*. Biomass and Bioenergy, 86, 76-87.

ULUSOY U. 2023, *A Review of Particle Shape Effects on Material Properties for Various Engineering Applications: From Macro to Nanoscale.* Minerals, 3, 91.

VANDERBRUGGEN A., SYGUSCH J., RUDOLPH M. ET AL. 2021, *A contribution to understanding the flotation behavior of lithium metal oxides and spheroidized graphite for lithium-ion battery recycling*. Colloids and Surfaces A: Physicochemical and Engineering Aspects, 626, 127111.

VAZIRI HASSAS B., CALISKAN H., GUVEN O. ET AL. 2016, *Effect of roughness and shape factor on flotation characteristics of glass beads.* Colloids and Surfaces A: Physicochemical and Engineering Aspects, 492, 88-99.

WU M., XIONG L., WANG J. 2021, *DEM study on effect of particle roundness on biaxial shearing of sand*. Underground Space 6, 678-694.

XU W., SUN K., QIU Y. ET AL. 2021, *Understanding the collection behavior of gangue minerals in fine flake graphite flotation.* Physicochemical Problems of Mineral Processing, DOI: 10.37190/ppmp/144408.

XU L., HU Y., DONG F. ET AL. 2017, *Crystal anisotropy of pegmatitic aluminosilicate minerals and its flotation application*. Beijing: Metallurgical Industry Press.

YAO F., LIU X., WU C. ET AL. 2022, P*reparation and Stability of Monodisperse Amorphous $CaCO_3$ Microspheres of High Hardness and Sphericity.* Inorg Chem; 61, 20150-20158.

YOU X. 2022, *Nanoparticle sphericity investigation of Cu-Al_2O_3-H_2O hybrid nanofluid flows between inclined channels filled with a porous medium*. Nanomaterials, 1, 413-426.

YANG B., YIN W., ZHU Z. ET AL. 2019, *A new model for the degree of entrainment in froth flotation based on mineral particle characteristics.* Powder Technology, 354, 358-368ZHOU N., CHENG X. 2016, *Research on the floatation process for large flake graphite ore in Inner Mongolia Autonomous Region.* Contemporary Chemical Industry, 45, 182-184, 188.

ZHOU S., WANG X., BU X. ET AL. 2020, *Effects of emulsified kerosene nanodroplets on the entrainment of gangue materials and selectivity index in aphanitic graphite flotation.* Minerals Engineering, 158, 106592.

ZHANG X., TAHMASEBI P. 2023, *Drafting, kissing and tumbling process of two particles: the effect of morphology.* International Journal of Multiphase Flow, 160, 104379.

ZHANG T., HUANG Q., GENG S. ET AL. 2023, *Impacts of solid physical properties on the performances of a slurry external airlift loop reactor integrating mixing and separation.* Chinese Journal of Chemical Engineering, 55, 1-12.

.